Control of Functional Responses Via Reversible Oxygen Loss in $La_{1-x}Sr_xFeO_{3-\delta}$ Films

*Yujun Xie, Mark D. Scafetta, Rebecca J. Sichel-Tissot, Eun Ju Moon, Robert C. Devlin, Hanqi Wu, Alex L. Krick, and Steven J. May**

The ability to control functional properties with external fields or stimuli is a major theme in oxide heterostructure research, with particular emphasis on functionalities not present in conventional semiconductors such as magnetism, ferroelectricity, correlated electron behavior, and first order electronic phase transitions. For example, substantial efforts are currently focused on switching magnetism with electric fields in magnetoelectrics[1–3] or controlling abrupt metal-insulator transitions with electrostatic gating.[4–8] An additional property of $ABO_{3-\delta}$ oxides, absent from conventional semiconductors, is the range of compositions that can be stabilized, with many oxides accommodating oxygen vacancy concentrations between $\delta = 0$–0.5. While the propensity for oxygen vacancies is largely viewed as a critical challenge in perovskite film synthesis,[9] the ability to dynamically control the oxygen composition in oxide heterostructures[10,11] may provide additional electronic or electrochemical device functionalities not accessible with conventional semiconductors as variations in anion composition can give rise to dramatic differences in macroscopic properties. For example, the room temperature electrical conductivity of metallic $LaNiO_3$ and insulating $LaNiO_{2.5}$ differs by over four orders of magnitude,[12] and the optical absorption coefficient of $LaNiO_{3-\delta}$ is sensitively dependent on δ.[13] Accessing these changes for functional devices requires dynamic control of oxygen composition. Temperature, electric field, or environment-induced changes to oxygen content have been studied extensively in bulk oxides, largely motivated by cathodic operation in solid oxide fuel cells[14–16] and the desire to identify materials for catalysis.[17,18] For instance, thermogravimetric analysis of bulk oxide ceramics has been used to demonstrate large changes in weight due to reduction and oxidation reactions (oxygen release and storage).[19–22] However, in such studies, the resultant effects on electronic structure are not reported and the temperatures for oxygen uptake and release are typically on the order of 400–500 °C for bulk ceramics. Further, the controlled coupling between anion composition and electrical properties has not been extensively studied in epitaxial heterostructures, which are the material architectures used for electronic devices.

Y. J. Xie, M. D. Scafetta, Dr. R. J. Sichel-Tissot, Dr. E. J. Moon, R. C. Devlin, H. Wu, A. Krick, Prof. S. J. May
Department of Materials Science and Engineering
Drexel University
Philadelphia, PA, 19104, USA
E-mail: smay@coe.drexel.edu

DOI: 10.1002/adma.201304374

Here we demonstrate reversible control of oxygen composition in $La_{1-x}Sr_xFeO_{3-\delta}$ (LSFO) epitaxial thin films at temperatures as low as 200 °C. Oxygen loss (reduction) within the films leads to an increase in room temperature resistivity of up to 6 orders of magnitude and a reduction in optical absorption. The effect is enhanced as the temperature is increased and film thickness is decreased. The changes to functional properties can be reversed by annealing in an O_3/O_2 mixture at 200 °C, allowing the films to be cycled between stoichiometric and oxgyen deficient compositions. This mechanism for optical and conduction modulation may serve as a platform for new devices or sensors in which external stimuli, electric fields or sample environment, are used to dynamically control the composition of complex oxide heterostructures.

$La_{1-x}Sr_xFeO_3$ films ($x \approx 0.7$, exact compositions can be found in the supplemental information) grown on $La_{0.18}Sr_{0.82}Al_{0.59}Ta_{0.41}O_3$ (LSAT) substrates are found to undergo dramatic changes in resistivity when heated in ambient environment at temperatures as low as 200 °C. **Figure 1**a displays the room temperature resistivity of a 39.5 nm thick LSFO film as a function of heating time at 200 °C. The resistivity increases by approximately two orders of magnitude after an hour; after five hours of heating time the film is over four orders of magnitude more resistive than in the nominally oxygen stoichiometric state. The film can be returned to the stoichiometric state by annealing in a mixed O_3/O_2 (~5/95%) environment at the same temperature of 200 °C for 30 minutes. The process can be cycled again by heating the sample at 200 °C in air to reduce the film, and subsequently reannealing in O_3/O_2 to oxidize the film. Surprised by this change in electronic properties due to low temperature heating in air, we next performed the same experiment on more commonly studied perovskite materials, $LaNiO_3$ and $La_{0.7}Sr_{0.3}MnO_3$, to determine how common the effect is among perovskites and to act as control experiments. Figure 1b shows the normalized room temperature resistivity of the three samples; no change in resistivity is observed for $LaNiO_3$ and $La_{0.7}Sr_{0.3}MnO_3$.

In addition to the change in resistivity, heating the film has the effect of turning it from dark brown and opaque to light yellow and translucent. The change in appearance is reflected in the optical absorption spectrum of the film as measured after heating in air and after the O_3/O_2 anneal, as shown in Figure 1c. The nominally oxygen stoichiometric film exhibits an absorption coefficient above 1.5×10^{-5} cm^{-1} over the measurement range of 1.2–5 eV, with broad absorption features centered at 2.9 and 4.1 eV. In contrast, the film heated in air shows a clear decrease (increase) in absorption at energies below (above) 3.4 eV.

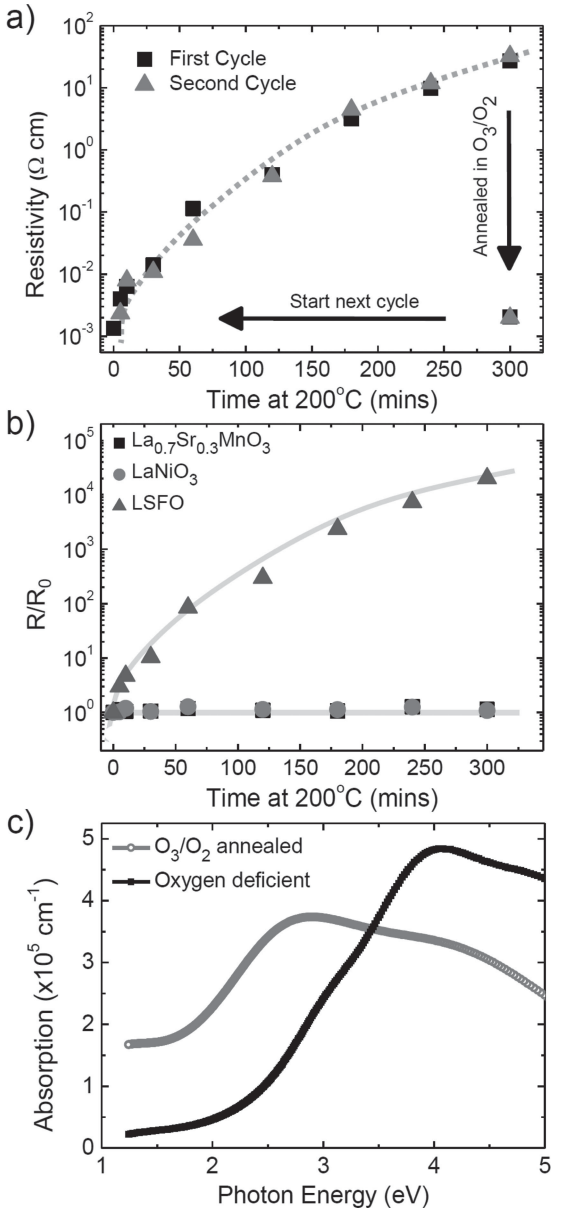

Figure 1. Resistivity in a 39.5 nm thick LSFO film as a function of time heated at 200 °C in air (a). The squares correspond to the first heating cycle, while the triangles correspond to the second heating cycle after the film had been reoxidized by annealing in a mixed O_3/O_2 environment at 200 °C. In (b), the normalized resistivity of the LSFO film is compared with other commonly studied conducting perovskite films, $La_{0.7}Sr_{0.3}MnO_3$ and $LaNiO_3$. The optical absorption for the LSFO film in the oxygen stoichiometric and deficient state is shown in (c).

We attribute the resistivity and absorption changes to a loss of oxygen content within the film, induced by heating in air. The Fe^{4+} valence state is unfavorable compared to the Fe^{3+} valence state, and LSFO has been shown to exhibit a propensity for oxygen vacancies, which act to compensate for the Sr doping on the La site thereby reducing the nominal iron valence state.[23–29] In bulk ferrites, the presence of oxygen vacancies is known to increase resistivity by orders of magnitude,[30] consistent with the present observation. Similarly, the absorption spectrum of the oxygen deficient film resembles that measured from $LaFeO_3$ films;[28] in both materials an increase in absorption near 2.5 eV and a strongly absorbing feature between 4.0 – 5.0 eV is observed. The observation that the spectrum of reduced LSFO is simliar to pure $LaFeO_3$ is consistent with an enhanced population of nominally Fe^{3+} cations induced by oxygen deficiency. An expansion of the lattice is an addition consequence of oxygen vacancies in LSFO that has been previously observed.[31,32]

The *c*-axis lattice parameter of the film was measured using x-ray diffraction after the various heating times to provide further confirmation of oxygen loss. **Figure 2**a presents the (002) diffraction peak measured from the 39.5 nm LSFO film during both the first and second heating cycle. The *c*-axis parameter of the film expands upon heating in atmosphere at 200 °C, increasing from 3.878 to 3.955 Å, as can be seen in Figure 2b. Similar to the resistivity, the *c*-axis parameter can be reduced back to 3.878 Å with the O_3/O_2 treatment. Despite the large structural change, thickness fringes persist in the diffraction data throughout the reduction and oxidation cycle of the film, indicating that the surface and interfacial morphologies are not degraded throughout the process. Figure 2c shows the relationship between the resistivity and the *c*-axis parameter obtained from two LSFO films, each ~39 nm thick.

While there is no readily available measurement technique capable of quantifying the oxygen composition in thin complex oxide films, we can obtain a rough estimate of the oxygen content by comparing the measured resistivity and lattice constants to previously reported values for bulk LSFO. Multiple groups have reported a room temperature resistivity of ~1×10^{-3} Ω-cm in bulk $La_{1/3}Sr_{2/3}FeO_3$.[33,34] This is the same value that we find in our oxygenated films on LSAT, indicating that the films after the O_3/O_2 anneal are nominally oxygen stoichiometric. Additionally, Blasco and coauthors measured a pseudocubic lattice volume of 58.04 $Å^3$ for $La_{1/3}Sr_{2/3}FeO_{2.99}$,[31] in excellent agreement with our measured values of ~58.03 $Å^3$ for the oxidized films. Zhou and Goodenough reported a room temperature resistivity of ~0.7 Ω-cm and a lattice volume of 58.31 $Å^3$ for bulk $La_{1/3}Sr_{2/3}FeO_{2.88}$.[35] These results suggests a *c*-axis parameter between 3.9 and 3.935 Å corresponds to an oxygen vacancy concentration of approximately 0.12 per formula unit for reduced LSFO on LSAT. The oxygen loss process is anticipated to terminate at an oxygen composition of $La_{0.3}Sr_{0.7}FeO_{2.65}$,[23] leading to a nominal 3+ valence on the iron cations and the removal of all 4+ sites. The resistivity of this compound has not been reported, although the crystal structure of $LaSr_2Fe_3O_8$ was studied and found to exhibit a brownmillerite-like structure in which oxygen vacancies order along every third FeO_2 plane with an average pseudocubic *c*-axis parameter of 3.962 Å.[36] This suggests that ordering of the vacancies is likely as the films become highly oxygen deficient; however, we have not observed Bragg reflections associated with this ordering, such as a (0 0 5/3) peak, in the reduced films. It is unclear if this is due to the weak intensity of such peaks making them unobservable with our diffractometer, or because the oxygen vacancies are not perfectly ordered over large enough length scales to give rise to coherent diffraction.

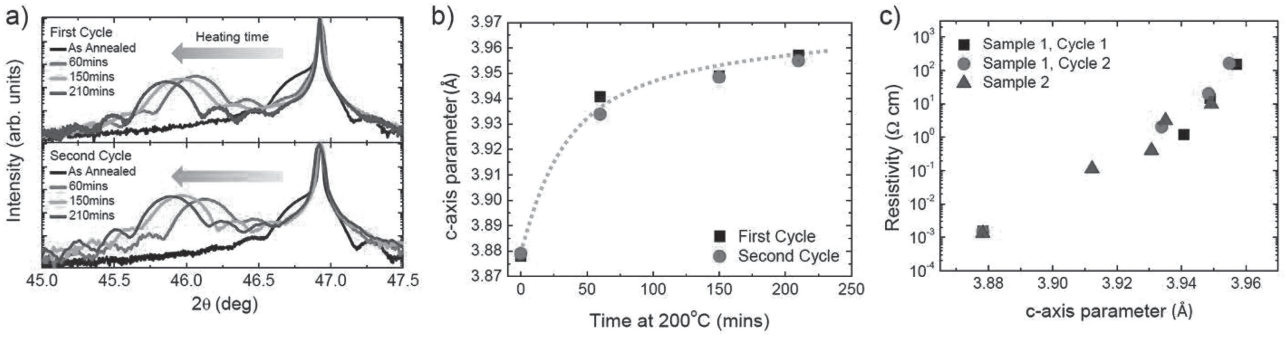

Figure 2. X-ray diffraction results measured for the 39.5 nm LSFO film (002) peak at various heating times (a). The LSAT (002) peak is at ~46.93°. The *c*-axis parameters for the film obtained from the diffraction data is presented in (b). In (c), the resistivity is plotted as a function of the *c*-axis parameter for two separate samples of comparable thickness.

To better understand the effect of oxygen loss on the electrical properties, variable temperature resistivity measurements were carried out on a 23.1 nm thick film throughout the heating process. The nominally oxygen stoichiometric film exhibits an increase in resistivity at 181 K, a feature observed in $La_{1-x}Sr_xFeO_3$ ($0.5 \leq x \leq 0.8$) that is attributed to charge disproportionation.[37] This transition appears to persist even after 40 min of heating, although the resistivity change at the transition becomes quite broad (**Figure 3**a). Interestingly, the transition temperature is relatively unchanged by the oxygen loss. At temperatures above the transition, the resistivity is best fit to a non-adiabatic polaron conduction mechanism, in which $\rho = \rho_0 T^{3/2} e^{E_A/kT}$, where k is Boltzmann's constant, E_A is the activation energy, and ρ_0 is the resistivity prefactor. The resistivity from 185 – 300 K was well described by this model for all heating times, as shown in Figure 3b. The obtained activation energies increase four fold over the first 120 min of heating before stabilizing at approximately 240 meV with longer heating times (Figure 3c), suggesting that the oxygen vacancies act to trap the polarons requiring increased thermal energy to move the carriers through the system. Our observation of polaronic transport is consistent with previous studies of bulk $La_{1-x}Sr_xFeO_3$ ($x \leq 0.3$) and reduced $La_{1/3}Sr_{2/3}FeO_{2.88}$.[35,38]

The oxygen loss can be accelerated by heating the film to 300 °C, as shown in **Figure 4**a for the 39.5 nm thick film, with 300 °C heating producing over 5 orders of magnitude higher resistivity than 200 °C heating after 1 hour. Further heating time at 300 °C results in resistance values that are too high for us to measure. The increased resistivity suggests that not only are the kinetics enhanced but the concentration of oxygen vacancies is also increased by heating at a higher temperature. A lower annealing temperature of 100 °C is insufficient to cause oxygen loss over the time scale of a few hours.

Reducing the film thickness provides an additional means to increase the speed of the oxygen loss process and the vacancy concentration. Figure 4b shows the room temperature resistivity for 4 different LSFO films as a function of heating time at 200 °C in atmosphere. The 6.9 nm thick film exhibits a resistivity increase of ~6 orders of magnitude in just 10 minutes, with further annealing it becomes too resistive to measure. The thickness dependence is systematic, as a 11.4 nm film exhibits slower kinetics than the 6.9 nm film, but faster kinetics compared to 16.5 and 39.5 nm films. The higher resistivities ($\geq 10^3$ Ω-cm) measured in thinner films and the film annealed at 300 °C likely indicate that the 16.5 and 39.5 nm films are not reduced to a state where the Fe cations are uniformly in the 3+ state, after 5 hours of heating at 200 °C.

The thickness dependence has important implications for creating devices, such as switches, sensors, or transistor-like devices, based on this phenomenon. For applications based on this effect, this result highlights how thinner films will lead to enhanced performance in the form of increased operating speed, on/off ratio, or sensing capabilities. One such envisioned device would consist of a heterojunction between LSFO and

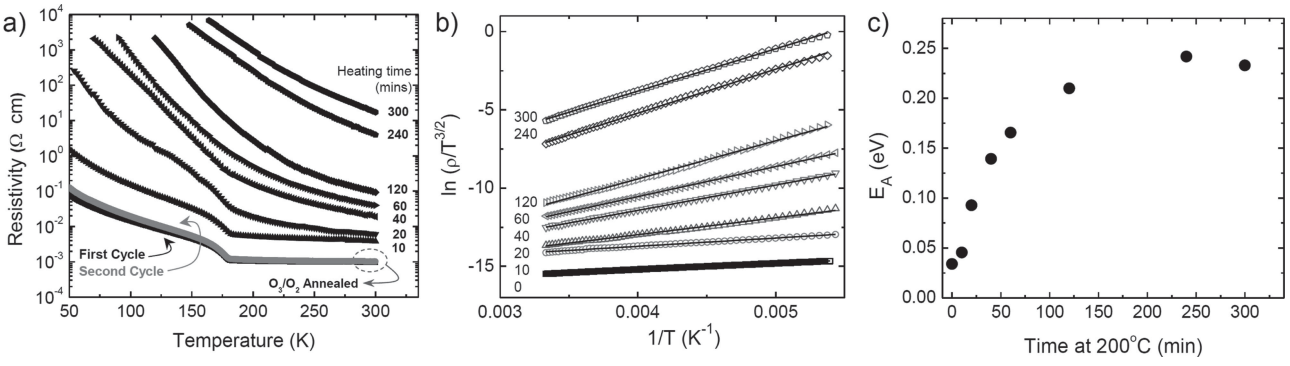

Figure 3. Temperature dependent resistivity measured from a 23.1 nm thick film as a function of different 200 °C annealing times (a). In (b), the resistivity data is shown fit to the polaron conduction model (solid lines). An increase in activation energy occurs upon reducing the films (c).

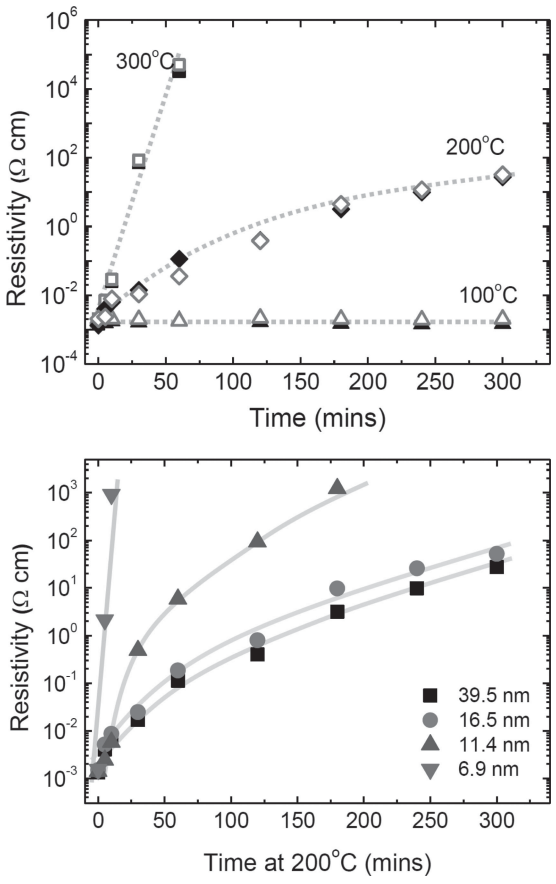

Figure 4. The effect of heating temperature on room temperature resistivity of the 39.5 nm film (a); the closed symbols indicate the first cycle, while the open symbols indicate the second cycle. The effect of film thickness on the room temperature resistivity change induced by oxygen loss is shown in (b).

an oxide that is an ionic conductor and electronic insulator. A cross-junction bias would be used to transport oxygen vacancies between the layers, modulating the conductivity in the LSFO. A transistor-like device based on a similar operating principle was recently demonstrated using a $SrTiO_3/CeO_2$:Gd junction.[39] Additionally, this result has consequences for the fabrication of devices based on metal-insulator transitions in complex oxides, such as ferrites (LSFO) or rare earth nickelates ($SmNiO_3$ or $EuNiO_3$) that are prone to oxygen deficiency. Processing steps, including hard bakes or metallization via vacuum deposition, in which the heterostructure is heated may lead to oxygen loss and a degradation of the electronic transition; indeed, it was during these procedures that we discovered the dramatic sensitivity to oxygen loss of LSFO.

In summary, we have demonstrated that reversible control of oxygen content at temperatures as low as 200 °C can induce dramatic changes to electronic conductivity, optical absorption, and lattice size in $La_{0.3}Sr_{0.7}FeO_{3-\delta}$ epitaxial films. The kinetics and magnitude of the effect can be enhanced by reducing the film thickness or increasing the temperature. We propose that dynamic control of oxygen content, achieved by electric fields,[8,16,39,40] electrochemical processes or ambient environment, may serve as a platform for electronic, optical, or sensing devices based on complex oxide heterostructures, with LSFO particularly well suited to such applications due to its ability to be reduced and oxidized at low temperatures.

Experimental Section

The oxide films were deposited using molecular beam epitaxy, in which the cations were evaporated from effusion cells and a 5/95 mixture of O_3/O_2 was used as the oxidizing environment. Growth temperatures and pressures were typically 575–650 °C and 2–8 × 10^{-6} Torr, respectively. Following growth, the LSFO films were annealed in a tube furnace under flowing O_3/O_2 (5/95%) at 200 °C for 30 min. This same procedure was used to reoxidize films after they had been reduced. X-ray diffraction and reflectivity measurements were performed using a Rigaku SmartLab instrument. The thickness of the films was determined by quantitative analysis of x-ray reflectivity data; the data and simulations (carried out using the GenX software package[41]) are shown in Figure S1, Supporting Information. The film compositions were determined based on Rutherford backscattering spectroscopy of films (Figure S2) grown simultaneously on MgO substrates. Film reduction was carried out by heating films in ambient environment on a hot plate; the hot plate temperature was verified by a thermocouple to be within ±3 °C of the set point temperature. Electrical resistivity of the films was measured in a Quantum Design Physical Properties Measurement System using external Keithley electronics to source current (model 6220) and measure voltage (model 2182A). Films were measured in a linear four point geometry with silver paint used to make contacts. After each room temperature resistivity measurement, the contacts were removed using acetone and IPA in ultrasonicator. The optical absorption spectra were obtained using a J.A. Woolam M-2000U variable angle spectroscopic ellipsometer. Details about the ellipsometry measurements and analysis methods can be found in Ref. [28].

Supporting Information

Supporting Information is available from the Wiley Online Library or from the author.

Acknowledgements

We thank Prof. Wei-Heng Shih for useful discussions. This work was supported by the Office of Naval Research (N00014–11–1–0664) and we acknowledge the Donors of the American Chemical Society Petroleum Research Fund for partial support of this research. X-ray diffraction was performed using the Centralized Research Facilities of the College of Engineering at Drexel University. The acquisition of the Physical Properties Measurement System was supported by the U. S. Army Research Office under grant number W911NF-11–1–0283.

Received: August 30, 2013
Published online: November 27, 2013

[1] Y.-H. Chu, L. W. Martin, M. B. Holcomb, M. Gajek, S.-J. Han, Q. He, N. Balke, C.-H. Yang, D. Lee, W. Hu, Q. Zhan, P.-L. Yang, A. Fraile-Rodríguez, A. Scholl, S. X. Wang, R. Ramesh, *Nat. Mater.* **2008**, *7*, 478.

[2] H. Béa, M. Gajek, M. Bibes, A. Barthélémy, *J. Phys.: Condens. Matter* **2008**, *20*, 434221.

[3] P. J. Ryan, J.-W. Kim, T. Birol, P. Thompson, J.-H. Lee, X. Ke, P. S. Normile, E. Karapetrova, P. Schiffer, S. D. Brown, C. J. Fennie, D. G. Schlom, *Nat. Commun.* **2013**, *4*, 1334.
[4] C. H. Ahn, A. Bhattacharya, M. Di Ventra, J. N. Eckstein, C. Daniel Frisbie, M. E. Gershenson, A. M. Goldman, I. H. Inoue, J. Mannhart, A. J. Millis, A. F. Morpurgo, D. Natelson, J.-M. Triscone, *Rev. Mod. Phys.* **2006**, *78*, 1185.
[5] R. Scherwitzl, P. Zubko, I. Gutierrez Lezama, S. Ono, A. F. Murpurgo, G. Catalan, J.-M. Triscine, *Adv. Mater.* **2010**, *22*, 5517.
[6] S. Asanuma, P.-H. Xiang, H. Yamada, H. Sato, I. H. Inoue, H. Akoh, A. Sawa, K. Ueno, H. Shimotani, H. Yuan, M. Kawasaki, Y. Iwasa, *Appl. Phys. Lett.* **2010**, *97*, 142110.
[7] M. Nakano, K. Shibuya, D. Okuyama, T. Hatano, S. Ono, M. Kawasaki, Y. Iwasa, Y. Tokura, *Nature* **2012**, *487*, 459.
[8] J. Jeong, N. Aetukuri, T. Graf, T. D. Schladt, M. G. Samant, S. S. P. Parkin, *Science* **2013**, *339*, 1402.
[9] S. A. Chambers, *Adv. Mater.* **2010**, *22*, 219.
[10] S. V. Kalinin, A. Borisevich, D. Fong, *ACS Nano* **2012**, *6*, 10423.
[11] S. V. Kalinin, N. A. Spaldin, *Science* **2013**, *341*, 858.
[12] R. D. Sánchez, M. T. Causa, A. Caneiro, A. Butera, M. Vallet-Regí, M. J. Sayagués, J. González-Calbet, F. García-Sanz, J. Rivas, *Phys. Rev. B* **1996**, *54*, 16574.
[13] B. Berini, N. Keller, B. Pigeau, Y. Dumont, E. Popova, N. Franco, R. M. C. Da Silva, *J. Appl. Phys.* **2008**, *104*, 113539.
[14] J. Mizusaki, N. Mori, H. Takai, Y. Yonemura, H. Minamiue, H. Tagawa, M. Dokiya, H. Inaba, K. Naraya, T. Sasamoto, T. Hashimoto, *Solid State Ionics* **2000**, *129*, 163.
[15] M. Oishi, K. Yashiro, K. Sato, J. Mizusaki, T. Kawada, *J. Solid State Chem.* **2008**, *181*, 3177.
[16] B. J. Ingram, J. A. Eastman, K.-C. Chang, S. K. Kim, T. T. Fister, E. Perret, H. You, P. M. Baldo, P. H. Fuoss, *Appl. Phys. Lett.* **2012**, *101*, 051603.
[17] E. Mamontov, T. Egami, R. Brezny, M. Koranne, S. Tyagi, *J. Phys. Chem. B* **2000**, *104*, 11110.
[18] H. Falcón, R. E. Carbonio, J. L. G. Fierro, *J. Catalysis* **2001**, *203*, 264.
[19] M. Machida, K. Kawamura, K. Ito, K. Ikeue, *Chem. Mater.* **2005**, *17*, 1487.
[20] S. Räsänen, T. Motohashi, H. Yamauchi, M. Karppinen, *J. Solid State Chem.* **2010**, *183*, 692.
[21] S. Remsen, B. Dabrowski, *Chem. Mater.* **2011**, *23*, 3818.
[22] T. Motohashi, Y. Hirano, Y. Masubuchi, K. Oshima, T. Setoyama, S. Kikkawa, *Chem. Mater.* **2013**, *25*, 372.
[23] J. Mizusaki, M. Yoshihiro, S. Yamauchi, K. Fueki, *J. Solid State Chem.* **1985**, *58*, 257.
[24] H. Yamada, M. Kawasaki, Y. Tokura, *Appl. Phys. Lett.* **2002**, *80*, 622.
[25] J. Cheng, A. Navrotsky, X.-D. Zhou, H. U. Anderson, *Chem. Mater.* **2005**, *17*, 2197.
[26] M. S gaard, P. Vang Hendriksen, M. Mogensen, *J. Solid State Chem.* **2007**, *180*, 1489.
[27] M. Reehuis, C. Ulrich, A. Maljuk, Ch. Niedermayer, B. Ouladdiaf, A. Hoser, T. Hofmann, B. Keimer, *Phys. Rev. B* **2011**, *85*, 184109.
[28] M. D. Scafetta, Y. J. Xie, M. Torres, J. E. Spanier, S. J. May, *Appl. Phys. Lett.* **2013**, *102*, 081904.
[29] A. M. Ritzmann, A. B. Munoz-García, M. Pavone, J. A. Keith, E. A. Carter, *Chem. Mater.* **2013**, *25*, 3011.
[30] T. Maeder, J. G. Bednorz, *J. Euro. Ceram. Soc.* **1999**, *19*, 1507.
[31] J. Blasco, M. C. Sánchez, J. García, J. Stankiewicz, J. Herrero-Martín, *J. Cryst. Growth* **2008**, *310*, 3247.
[32] X. Chen, T. Grande, *Chem. Mater.* **2013**, *25*, 3296.
[33] S. K. Park, T. Ishikawa, Y. Tokura, J. Q. Li, Y. Matsui, *Phys. Rev. B* **1999**, *60*, 10788.
[34] J. Blasco, B. Aznar, J. García, G. Subías, J. Herrero-Martín, J. Stankiewicz, *Phys. Rev. B* **2008**, *77*, 054107.
[35] H. D. Zhou, J. B. Goodenough, *J. Solid State Chem.* **2005**, *178*, 3679.
[36] P. D. Battle, T. C. Gibb, P. Lightfoot, *J. Solid State Chem.* **1990**, *84*, 237.
[37] J. Matsuno, T. Mizokawa, A. Fujimori, K. Mamiya, Y. Takeda, S. Kawasaki, M. Takano, *Phys. Rev. B* **1999**, *60*, 4605.
[38] W. H. Jung, E. Iguchi, *J. Phys.: Condens. Matter* **1995**, *7*, 1215.
[39] T. Tsuchiya, K. Terabe, M. Aono, *Appl. Phys. Lett.* **2013**, *103*, 073110.
[40] D. N. Leonard, A. Kumar, S. Jesse, M. D. Biegalski, H. M. Christen, E. Mutoro, E. J. Crumlin, Y. Shao-Horn, S. V. Kalinin, A. Y. Borisevich, *Adv. Energy Mater.* **2013**, *3*, 788.
[41] M. Bjorck, G. Andersson, *J. Appl. Crystallogr.* **2007**, *40*, 1174.